Plant Communications
Research article

CellPress
Partner Journal

ESR2–HDA6 complex negatively regulates auxin biosynthesis to delay callus initiation in *Arabidopsis* leaf explants during tissue culture

Kyounghee Lee[1,2], Hobin Yoon[3], Ok-Sun Park[4], Jongbu Lim[5], Sang-Gyu Kim[5] and Pil Joon Seo[1,2,3,4,*]

[1]Department of Chemistry, Seoul National University, Seoul 08826, Korea

[2]Research Institute of Basic Sciences, Seoul National University, Seoul 08826, Korea

[3]Interdisciplinary Program in Agricultural Biotechnology, Seoul National University, Seoul 08826, Korea

[4]Plant Genomics and Breeding Institute, Seoul National University, Seoul 08826, Korea

[5]Department of Biological Sciences, KAIST, Daejeon 34141, Korea

***Correspondence: Pil Joon Seo (pjseo1@snu.ac.kr)**

https://doi.org/10.1016/j.xplc.2024.100892

ABSTRACT

Plants exhibit an astonishing ability to regulate organ regeneration upon wounding. Excision of leaf explants promotes the biosynthesis of indole-3-acetic acid (IAA), which is polar-transported to excised regions, where cell fate transition leads to root founder cell specification to induce *de novo* root regeneration. The regeneration capacity of plants has been utilized to develop *in vitro* tissue culture technologies. Here, we report that IAA accumulation near the wounded site of leaf explants is essential for callus formation on 2,4-dichlorophenoxyacetic acid (2,4-D)-rich callus-inducing medium (CIM). Notably, a high concentration of 2,4-D does not compensate for the action of IAA because of its limited efflux; rather, it lowers IAA biosynthesis via a negative feedback mechanism at an early stage of *in vitro* tissue culture, delaying callus initiation. The auxin negative feedback loop in CIM-cultured leaf explants is mediated by an auxin-inducible APETALA2 transcription factor, ENHANCER OF SHOOT REGENERATION 2 (ESR2), along with its interacting partner HISTONE DEACETYLASE 6 (HDA6). The ESR2–HDA6 complex binds directly to, and removes the H3ac mark from, the *YUCCA1* (*YUC1*), *YUC7*, and *YUC9* loci, consequently repressing auxin biosynthesis and inhibiting cell fate transition on 2,4-D-rich CIM. These findings indicate that negative feedback regulation of auxin biosynthesis by ESR2 and HDA6 interferes with proper cell fate transition and callus initiation.

Key words: auxin biosynthesis, negative feedback loop, ESR2, HDA6, YUCCA, chromatin modification

Lee K., Yoon H., Park O.-S., Lim J., Kim S.-G., and Seo P.J. (2024). ESR2–HDA6 complex negatively regulates auxin biosynthesis to delay callus initiation in *Arabidopsis* leaf explants during tissue culture. Plant Comm. **5**, 100892.

INTRODUCTION

Plants have a remarkable ability to regenerate new tissues, organs, and even whole plantlets, especially after wounding (Yu et al., 2017b; Iwase et al., 2017; Ikeuchi et al., 2020). Among the various types of organs regenerated from wounded tissues, regeneration of adventitious roots from leaf explants has been extensively investigated in *Arabidopsis thaliana* (Liu et al., 2014, 2022; Chen et al., 2016; Hu and Xu, 2016). Wounding stress promotes auxin biosynthesis and polar auxin transport in leaf explants, thereby establishing a local auxin maximum at the excised region (Chen et al., 2016). Auxin accumulation at the wound site is essential for the transition of regeneration-competent cells into root founder cells via the activation of *WUSCHEL-RELATED HOMEOBOX 11* (*WOX11*) (Liu et al., 2014; Hu and Xu, 2016). Cell division subsequently occurs to facilitate the transition from root founder cells to root primordium cells, which is marked by *WOX5* expression (Hu and Xu, 2016). Ultimately, adventitious roots are generated from the root primordium (Liu et al., 2014; Hu and Xu, 2016). Blocking the biosynthesis or polar transport of auxin leads to the loss of auxin maximum in wound-adjacent competent cells, inhibiting *de novo* root regeneration (Liu et al., 2014; Chen et al., 2016).

Published by the Plant Communications Shanghai Editorial Office in association with Cell Press, an imprint of Elsevier Inc., on behalf of CSPB and CEMPS, CAS.

The regeneration ability of plants has been exploited for *in vitro* tissue culture (Sussex, 2008). Similar to the role of auxin in establishing root primordium identity during *de novo* root regeneration, incubation on 2,4-dichlorophenoxyacetic acid (2,4-D)-rich callus-inducing medium (CIM) allows efficient formation of pluripotent callus, with root primordium characteristics, near the wound site (Liu et al., 2018; Shin and Seo, 2018). During callus formation on CIM, a subset of LATERAL ORGAN BOUNDARIES DOMAIN transcription factors is activated, which facilitates the acquisition of root primordium identity in callus (Fan et al., 2012). Furthermore, PLETHORA 3 (PLT3), PLT5, and PLT7 activate root meristem identity genes, such as *PLT1* and *PLT2*, in calli to establish competence for organogenesis (Kareem et al., 2015). After the acquisition of pluripotency, the callus is usually transferred to shoot-inducing medium to stimulate *de novo* shoot organogenesis (Che et al., 2007). In the course of *de novo* shoot formation from callus cells, the type B ARABIDOPSIS RESPONSE REGULATOR–WUSCHEL module acts as a key regulator of shoot progenitor formation (Meng et al., 2017). Two APETALA2/ETHYLENE RESPONSE FACTOR-type transcriptional activators, DORNROSCHEN (DRN)/ENHANCER OF SHOOT REGENERATION 1 (ESR1) and DRN-LIKE/ESR2, also promote shoot regeneration (Matsuo et al., 2011; Temman et al., 2023). Accumulating evidence indicates that many genetic components involved in the plant regeneration process are intricately linked in both callus formation and *de novo* shoot organogenesis, thereby coordinating cell fate transition for efficient *in vitro* tissue culture (Liu et al., 2018; Lee et al., 2021).

Callus initiation in several plant species continues to pose challenges (Hu et al., 2017; Ghanbari et al., 2018). For example, callus initiation is difficult when using the mature vegetative organs of several monocot plants, including rice and maize (Hu et al., 2017). Our knowledge of the molecular mechanism that underlies the initial cell fate transition during callus formation is limited; thus, it is important to elucidate the initial process of cell fate transition and to identify the genetic barrier that interferes with this biological process. Despite the lack of empirical evidence, *de novo* root organogenesis and callus formation from leaf explants are suspected to share the initial process of cellular reprogramming in *Arabidopsis*, which potentially involves the accumulation of a natural auxin, indole-3-acetic acid (IAA), at the wound site (Liu et al., 2014). After the shared initial step of root founder cell formation, *de novo* root organogenesis and callus formation are thought to diverge, depending on exogenous auxin treatment: the absence of exogenous auxin leads to *de novo* root regeneration, whereas the application of high exogenous 2,4-D treatment induces the formation of proliferating callus with root characteristics, instead of adventitious roots, particularly in *Arabidopsis* leaf explants (Yu et al., 2017b).

Auxin is synthesized via both tryptophan-dependent and tryptophan-independent pathways in plants (Zhao et al., 2002). Among others, YUCCA (YUC) flavin monooxygenases that oxidize tryptamine to N-hydroxytryptamine are well-characterized catalytic enzymes involved in *de novo* tryptophan-dependent auxin biosynthesis (Zhao et al., 2002). The *Arabidopsis* genome contains 11 *YUC* (*YUC1–YUC11*) genes (Cao et al., 2019), which exhibit variable temporal and spatial expression patterns and control various plant developmental processes (Bai et al., 2013; Cai et al., 2014; Challa et al., 2016). It is noteworthy that YUC-mediated auxin biosynthesis is regulated by a negative feedback mechanism (Suzuki et al., 2015): high auxin accumulation and signaling suppress a subset of *YUC* genes via an unknown mechanism, which inhibits auxin biosynthesis to maintain auxin homeostasis (Suzuki et al., 2015).

In this study, we report that 2,4-D-triggered negative feedback regulation of *YUC* genes limits cell fate transition, thereby delaying callus initiation on 2,4-D-containing CIM (2,4-D-CIM) during tissue culture. The initial cell fate transition at the wound site requires IAA accumulation, which is established by endogenous auxin biosynthesis and transport. However, 2,4-D treatment of *in vitro* tissue culture fails to mimic IAA action because it lacks an efflux mechanism and even represses IAA biosynthesis via feedback regulation, thereby delaying cell fate transition and subsequent callus formation. This negative feedback regulation of auxin biosynthesis is mediated by the auxin-activated ESR2–HISTONE DEACETYLASE 6 (HDA6) complex. Mutations in *ESR2* and *HDA6* impair the negative feedback loop, allowing efficient cell fate transition and callus initiation, even on 2,4-D-CIM. These results indicate that chromatin-dependent regulation underlies the negative feedback control of auxin biosynthesis, serving as a genetic barrier to *in vitro* tissue culture.

RESULTS

Endogenous auxin is required for callus initiation during tissue culture

Endogenous auxin is essential for the initial cell fate transition during *de novo* root organogenesis (Chen et al., 2016). A local maximum of endogenous auxin at the wound site, based on polar auxin transport, is particularly important for establishing root founder cells (Liu et al., 2014; Chen et al., 2016). Given that callus formation largely follows *de novo* root regeneration (Liu et al., 2014), we asked whether endogenous auxin-dependent cell fate transition is also required for callus initiation on 2,4-D-CIM. Leaf explants were incubated on 2,4-D-CIM supplemented with or without a potent inhibitor of IAA-biosynthetic YUC enzymes, yucasin difluorinated analog (YDF) (5-[2,6-difluorophenyl]-2,4-dihydro-[1,2,4]-triazole-3-thione) (Tsugafune et al., 2017) (Supplemental Figure 1). Even in the presence of a high concentration of 2,4-D, YDF treatment considerably inhibited cell fate transition, as indicated by the reduction in *WOX11* marker gene expression (Figure 1A and 1B). Unlike a canonical auxin marker gene, reduction of *WOX11* expression indicates cell fate transition into root founder cells (Liu et al., 2014), (Supplemental Figure 2). Given that the reduced cell fate transition by YDF treatment was restored by IAA application (Supplemental Figure 2), it suggests that the initial cell fate transition requires IAA biosynthesis, a process not adequately substituted by 2,4-D application. Consequently, callus formation was also substantially inhibited by YDF treatment (Figure 1C and 1D). The reduced callus size was caused by delayed cell fate initiation (Figure 1A, 1B, 1E, and 1F) rather than reduced callus proliferation, as YDF treatment during the callus proliferation stage did not influence callus size (Supplemental Figure 3). To further validate this result, we employed the *yuc2589* mutant, which shows defects in auxin biosynthesis (Boccaccini et al., 2020), to examine callus formation on 2,4-D-CIM. Consistent with our hypothesis, the *yuc2589* mutant showed significantly

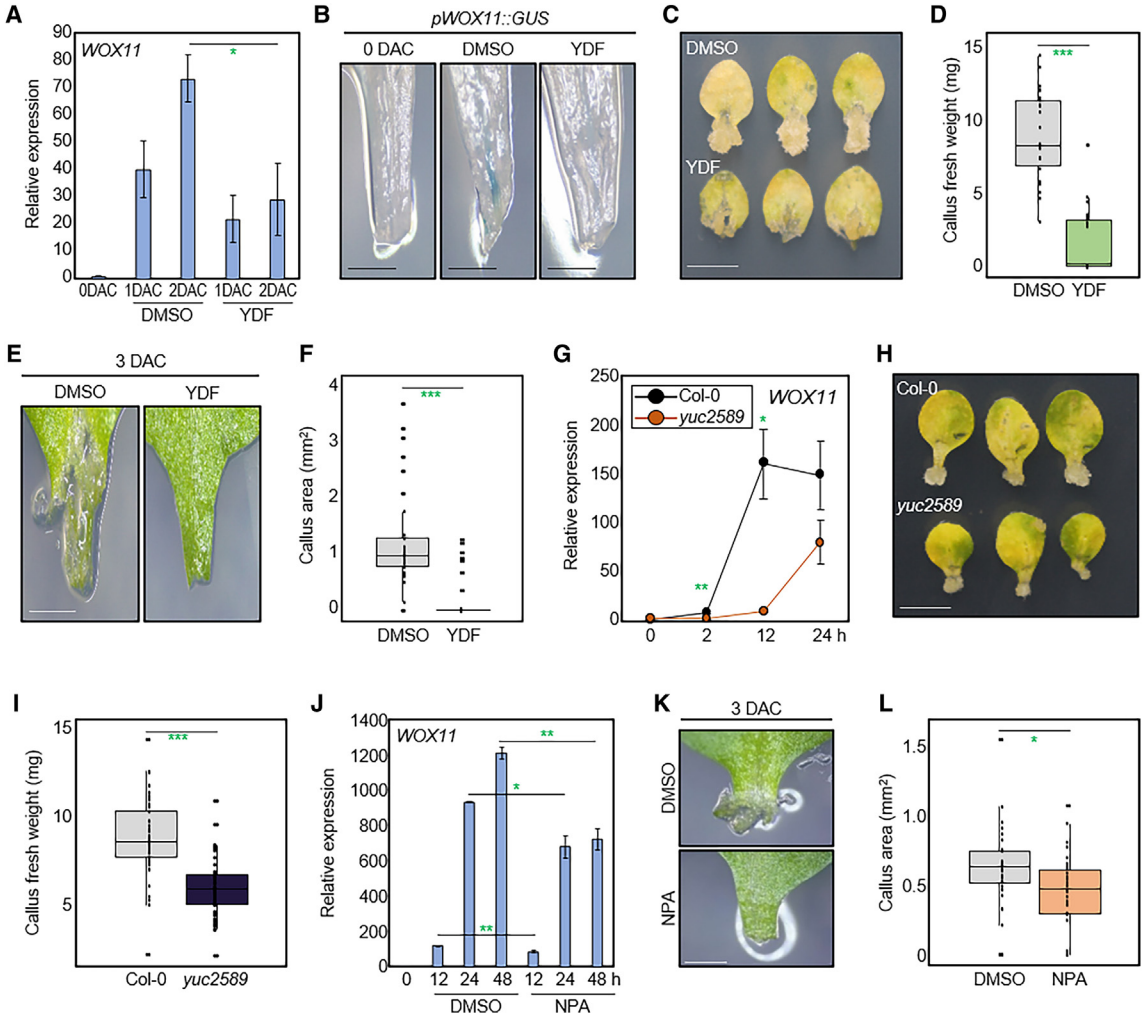

Figure 1. Endogenous auxin is required for callus formation.

(A) Effects of YDF on the transition of regeneration-competent cells into root founder cells during *in vitro* tissue culture. Leaf explants from 2-week-old plants were incubated for up to 2 days on 2,4-D-CIM supplemented with 200 μM YDF. The wound site of leaf explants, showing *WOX11* expression, was selectively harvested for gene expression analysis. The transcript level of *WOX11* was analyzed by real-time RT-qPCR. The *eIF4a* gene (At3g13920) was used as an internal control.

(B) *WOX11* promoter activity in *pWOX11::GUS* transgenic leaf explants cultured on 2,4-D-CIM supplemented with 200 μM YDF for 2 days. Scale bars, 1 mm.

(C) Callus formation in leaf explants incubated on 2,4-D-CIM supplemented with 400 μM YDF for 2 weeks. Scale bar, 5 mm.

(D) Callus fresh weight measurement.

(E) Callus initiation phenotype of leaf explants incubated on 2,4-D-CIM supplemented with 400 μM YDF for 3 days. Scale bar, 1 mm.

(F) Callus area measurement. Area of callus that emerged at leaf wound sites was quantified by ImageJ.

(G) *WOX11* expression at the wound site of *yuc2589* mutant leaf explants after incubation on 2,4-D-CIM for up to 24 h.

(H) Callus formation in *yuc2589* mutant leaf explants incubated on 2,4-D-CIM for 2 weeks. Scale bar, 5 mm.

(I) Fresh weight of wild-type and *yuc2589* mutant calli.

(J) Effects of NPA on the transition of regeneration-competent cells into root founder cells. Leaf explants were incubated on 2,4-D-CIM supplemented with 50 μM NPA for up to 48 h. The wound site of leaf explants was selectively harvested for gene expression analysis.

(K) Callus initiation phenotype on 2,4-D-CIM supplemented with 50 μM NPA at 3 DAC. Scale bar, 1 mm.

(L) Callus area measurement. Area of callus that emerged at leaf wound sites was quantified by ImageJ. Data in **(A), (G), and (J)** represent the mean ± SEM of three biological replicates, whereas data in **(D), (F), (I), and (L)** represent box-and-whisker plots. Asterisks indicate statistically significant differences (*$P < 0.05$, **$P < 0.01$, ***$P < 0.001$; Student's *t*-test). DAC, days after incubation on 2,4-D-CIM.

delayed cell fate transition and reduced *WOX11* expression (Figure 1G). Callus fresh weight of the *yuc2589 mutant* was reduced by 33% on 2,4-D-CIM compared with that of the wild type (Figure 1H and 1I), suggesting that 2,4-D does not mimic the effect of IAA during the initial cell fate transition. The IAA-dependent cell fate transition was only relevant in leaf explants, as *WOX11* expression remained unaffected during callus initiation in hypocotyl and root explants of the *yuc2589* mutant (Supplemental Figure 4). Callus fresh weight was also comparable between wild type and *yuc2589* mutant calli

derived from hypocotyl or root explants (Supplemental Figure 4). Consistently, YDF treatment also had no impact on *WOX11* promoter activity in hypocotyl and root explants (Supplemental Figure 5).

The main difference between endogenous auxin (IAA) and exogenously applied synthetic auxin (2,4-D) lies in their polar transport mechanisms: IAA is polar-transported by auxin efflux carriers (PIN-FORMED [PIN] proteins), whereas 2,4-D is not transported by PINs (Parizkova et al., 2021). Thus, we examined the effect of naphthylphthalamic acid (NPA), which specifically blocks endogenous auxin transport without affecting exogenous auxin treatment (Teale and Palme, 2018), on callus initiation during incubation on 2,4-D-CIM. NPA treatment substantially delayed cell fate transition and subsequent callus initiation (Figure 1J–1L); however, the application of NPA during callus proliferation did not affect callus size (Supplemental Figure 6). These results suggest that both auxin biosynthesis and accumulation near wound sites are critical for cell fate transition during the callus initiation stage in *in vitro* tissue culture.

Exogenous 2,4-D treatment delays cell fate transition and callus initiation

Negative feedback regulation of auxin biosynthesis has been reported (Suzuki et al., 2015), and exogenous treatment with synthetic auxins, including 2,4-D, naphthalene-1-acetic acid (NAA), and picloram, inhibits IAA biosynthesis by reducing *YUC* expression to maintain auxin homeostasis (Suzuki et al., 2015) (Supplemental Figure 7). We therefore suspected that not only did the exogenously applied 2,4-D fail to compensate for the role of IAA in cell fate transition (Figure 1), but 2,4-D treatment may also lower IAA biosynthesis via the negative feedback circuit, suppressing cell fate transition for callus initiation. The *YUC* genes were specifically expressed in the midvein regions before 2,4-D application (Chen et al., 2016) (Supplemental Figure 9). Consistent with our hypothesis, the expression of *YUC* genes was suppressed in leaf explants incubated on 2,4-D-CIM compared with those incubated on 2,4-D-depleted CIM (Figure 2A; Supplemental Figure 8). In line with this result, the level of free IAA was also reduced in leaf explants cultured on 2,4-D-CIM compared with those cultured on 2,4-D-depleted CIM (Ohbayashi et al., 2022) (Figure 2B).

These observations prompted us to examine the possibility that treatment with 2,4-D, which does not mimic IAA action in cell fate transition and even lowers IAA biosynthesis via a negative feedback mechanism, inhibits callus initiation at wound sites. Indeed, independent of 2,4-D concentration, incubation of leaf explants on 2,4-D-CIM delayed cell fate transition, with reduced *WOX11* expression, compared with incubation on 2,4-D-depleted CIM (Figure 2C and 2D), (Supplemental Figure 10). In agreement with these observations, expression of the *ARF7* gene, which is essential for callus initiation, was also delayed in calli incubated on 2,4-D-CIM (Figure 2E). The delayed cell fate transition of calli cultured on 2,4-D-CIM was rescued by treatment with IAA, but not by another synthetic auxin (Figure 2F and 2G). Overall, the synthetic auxin 2,4-D reduces IAA biosynthesis via a negative feedback mechanism, delaying the initial cell fate transition, although 2,4-D enables robust callus proliferation at later stages following the cell fate transition (Xu et al., 2018) (see discussion).

Taken together, these results suggest that the *in vitro* tissue culture method involving high-level synthetic auxin treatment intrinsically affects callus initiation by altering endogenous auxin biosynthesis in leaf explants (Figure 2H).

HDA6 negatively regulates *YUC1*, *YUC7*, and *YUC9* expression in calli incubated on 2,4-D-CIM

We found that suppression of auxin biosynthesis via a negative feedback mechanism limits callus initiation during *in vitro* tissue culture. To override this negative feedback loop, which would be rapidly activated upon incubation on 2,4-D-CIM, we decided to unravel its molecular basis by searching for auxin-inducible genes that are known to attenuate auxin signaling. The *HDA6* gene was of particular interest, as it was highly upregulated by exogenous 2,4-D treatment (Supplemental Figure 11) and is known to repress auxin signaling (Wojcikowska et al., 2018). Consistent with its induction by exogenous 2,4-D treatment, the expression of *HDA6* was also induced by incubation on 2,4-D-CIM (Figure 3A and 3B), especially in vascular tissues (Figure 3C; Supplemental Figure 11), where the *YUC* genes were mainly suppressed following incubation on 2,4-D-CIM (Figure 2A).

To investigate the role of *HDA6* in endogenous auxin biosynthesis on 2,4-D-CIM, we obtained an *HDA6*-deficient mutant, *hda6-6*. The leaf explants of *hda6-6* and the wild type were cultured on 2,4-D-CIM, and the expression of auxin biosynthesis genes was analyzed. Notably, *YUC1*, *YUC7*, and *YUC9* were specifically and significantly upregulated in *hda6-6* compared with the wild type (Figure 3D), particularly in the midvein regions (Supplemental Figure 12). Next, to test whether HDA6 binds directly to the *YUC1*, *YUC7*, and *YUC9* loci, we performed a chromatin immunoprecipitation–quantitative PCR (ChIP-qPCR) assay on 35S:*MYC-HDA6* leaf explants cultured on 2,4-D-CIM using an anti-MYC antibody. The results revealed that HDA6 specifically associated with *YUC1*, *YUC7*, and *YUC9* chromatin near the transcription start site and in the gene body (Figure 3E and 3F). Given that HDA6 removes acetyl groups from histone H3 molecules (Yu et al., 2011), we examined H3 acetylation levels at the *YUC* loci in *hda6-6* mutant leaf explants. Notably, H3 acetylation levels were substantially elevated at *YUC1*, *YUC7*, and *YUC9* loci in *hda6-6* leaf explants (Figure 3G). In addition to the binding site of HDA6, we observed occasional increases in H3 acetylation levels at neighboring regions on the *YUC* loci in *hda6-6* (Figure 3G).

Endogenous IAA is critical for cell fate transition to subsequently induce callus. Therefore, we speculated that the *hda6-6* mutant displays enhanced cell fate transition because of its higher IAA content compared with the wild type. Indeed, root founder cell and root primordium marker genes were rapidly activated in *hda6-6* leaf explants cultured on 2,4-D-CIM (Supplemental Figure 13), indicating earlier cell fate transition in *hda6-6*. Because of the earlier initiation of callus proliferation, the size of *hda6-6* leaf explant-derived calli was significantly larger than that of wild-type leaf explant-derived calli at 14 days after incubation on 2,4-D-CIM (DAC) (Supplemental Figure 14). The fresh weight of *hda6-6* calli was 25% greater than that of wild-type calli at 14 DAC (Supplemental Figure 14), which could be reversed by the expression of GFP-tagged *HDA6* driven by the native promoter (Supplemental Figure 15). To further confirm whether the larger *hda6-6* callus size was due

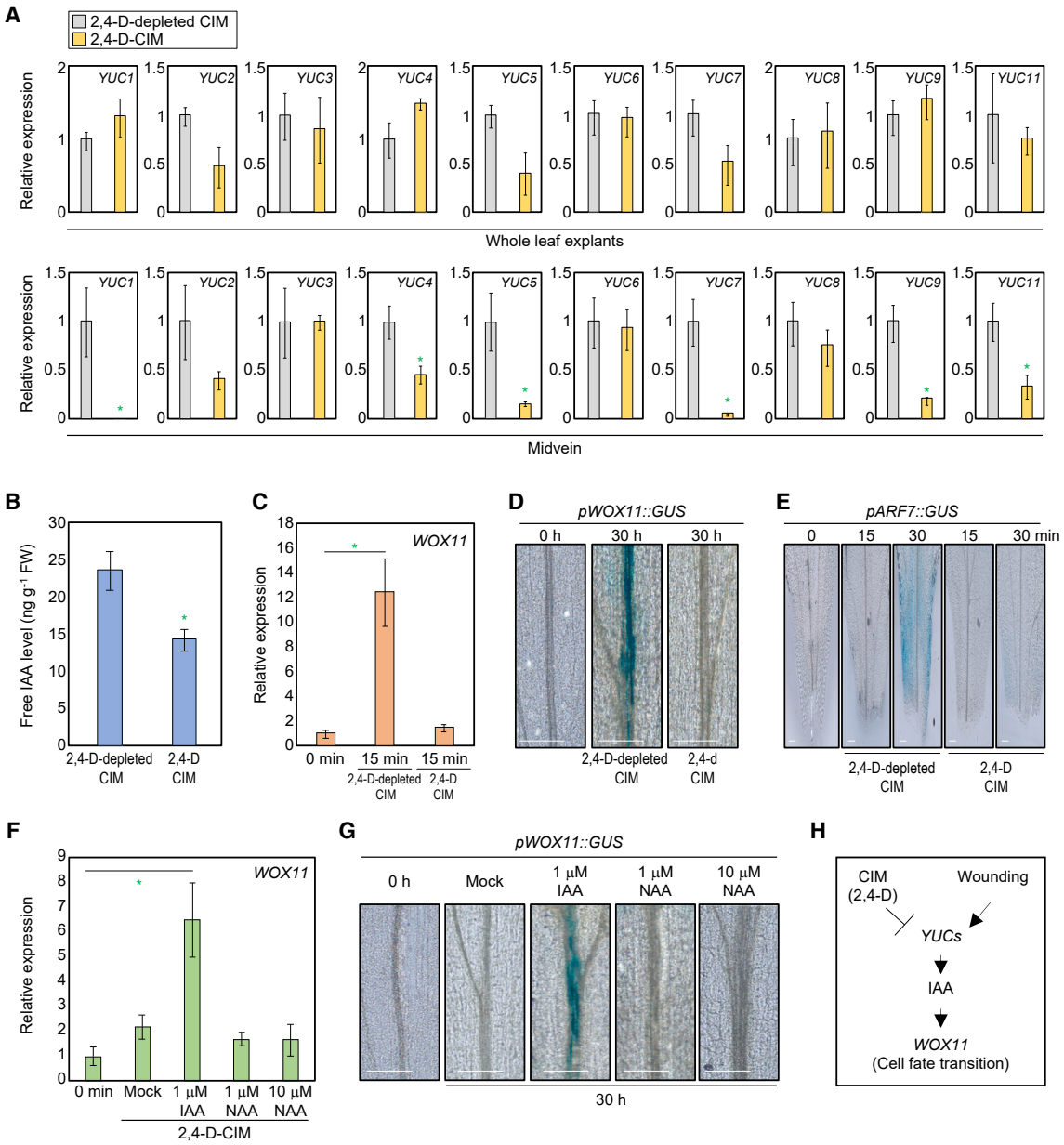

Figure 2. *YUC* expression is repressed in leaf explants cultured on 2,4-D-CIM.

(A) Expression of *YUC* genes in leaf explants incubated on 2,4-D-CIM or 2,4-D-depleted CIM for 24 h. Whole leaf explants were harvested for real-time RT-qPCR (top). Midvein samples (bottom) were prepared as shown in Supplemental Figure 8.

(B) Measurement of free IAA content in leaf explants incubated on 2,4-D-CIM or 2,4-D-depleted CIM for 24 h.

(C) Real-time RT-qPCR analysis of *WOX11* expression in leaf explants incubated on 2,4-D-CIM or 2,4-D-depleted CIM for 15 min. The wound site of leaf explants, showing *WOX11* expression, was selectively harvested for gene expression analysis.

(D) Spatial expression of *WOX11*. The *pWOX11::GUS* transgenic leaf explants were incubated on 2,4-D-CIM or 2,4-D-depleted CIM for 30 h. Scale bars, 200 μm.

(E) *ARF7* expression in *pARF7::GUS* transgenic leaf explants incubated on 2,4-D-CIM or 2,4-D-depleted CIM for up to 30 min. Scale bars, 200 μm.

(F) Real-time RT-qPCR analysis of *WOX11* expression in leaf explants incubated on 2,4-D-CIM supplemented with 1 μM IAA, 1 μM NAA, or 10 μM NAA for 45 min. The wound site of leaf explants, showing *WOX11* expression, was selectively harvested for gene expression analysis.

(G) *WOX11* expression in the midvein regions of *pWOX11::GUS* transgenic leaf explants incubated on 2,4-D-CIM supplemented with 1 μM IAA, 1 μM NAA, or 10 μM NAA for 30 h. Scale bars, 200 μm.

(H) Schematic representation showing the role of 2,4-D in delaying cell fate transition. Data in **(A), (B), (C), and (F)** represent the mean ± SEM of three biological replicates. Asterisks indicate statistically significant differences (*$P < 0.05$; Student's *t*-test).

to its higher IAA level, we performed YDF treatment. The results showed that YDF reversed the enhanced cell fate transition and callus initiation of *hda6-6* (Supplemental Figures 14 and 16), demonstrating that HDA6 inhibits auxin biosynthesis and thereby delays cell fate transition and callus initiation on 2,4-D-CIM.

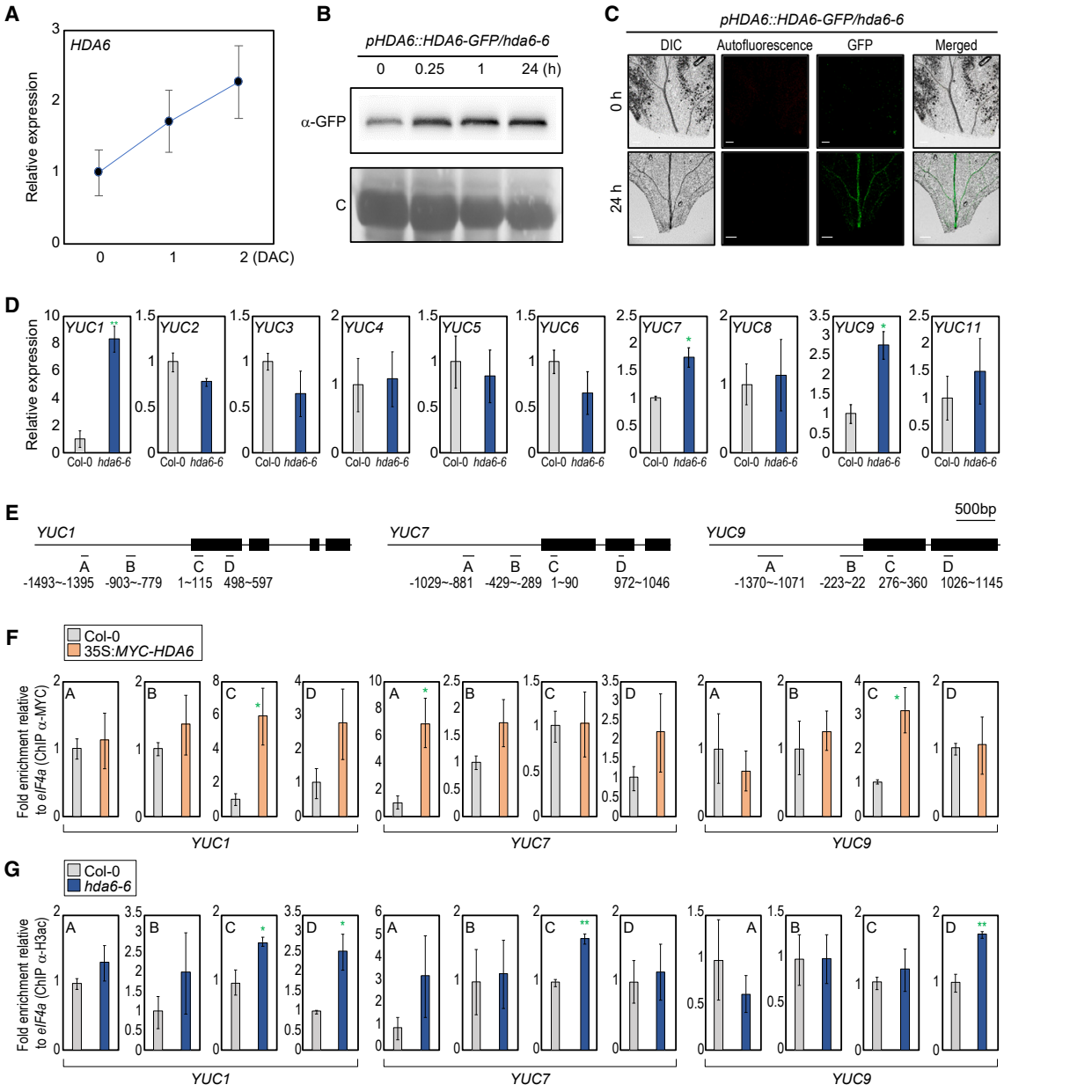

Figure 3. HDA6 directly represses *YUC1*, *YUC7*, and *YUC9* expression.

(A) *HDA6* expression in leaf explants incubated on 2,4-D-CIM for up to 2 days. Whole leaf explants were used for gene expression analysis.

(B) HDA6 protein level in *pHDA6::HDA6-GFP/hda6-6* transgenic leaf explants incubated on 2,4-D-CIM. h, hours after incubation on 2,4-D-CIM.

(C) HDA6 protein activity in *pHDA6::HDA6-GFP/hda6-6* leaf explants cultured on 2,4-D-CIM. Scale bars, 100 μm.

(D) Expression of *YUC* genes in wild-type and *hda6-6* leaf explants from 2-week-old plants cultured on 2,4-D-CIM for 50 min.

(E) Structure of *YUC1*, *YUC7*, and *YUC9* genes. Black lines above the labels indicate regions amplified by quantitative PCR (qPCR) following chromatin immunoprecipitation (ChIP). Black boxes indicate exons.

(F) Enrichment of HDA6 on *YUC* loci. Values obtained from control plants were set to 1 after normalization against *eIF4a*.

(G) Abundance of H3ac at *YUC1*, *YUC7*, and *YUC9* loci in wild-type and *hda6-6* mutants, as analyzed by ChIP-qPCR using an anti-H3ac antibody. Data in **(A), (D), (F), and (G)** indicate the mean ± SEM of three biological replicates. Asterisks indicate statistically significant differences (*$P < 0.05$, **$P < 0.01$; Student's *t*-test).

HDA6 interacts with ESR2

Given that HDA6 has no DNA-binding selectivity to the *YUC1*, *YUC7*, and *YUC9* loci, we hypothesized that HDA6 may rely on another transcription factor, which binds to DNA in a sequence-specific manner, to control *YUC* expression. To identify HDA6-interacting proteins, we carried out yeast two-hybrid (Y2H) screening using a commercial cDNA library (Matiolli and Melotto, 2018). Preliminary results suggested that HDA6 interacts with ESR2, which is involved in *in vitro* plant regeneration (Ikeda et al., 2006, 2021; Nag et al., 2007; Matsuo et al., 2011). To validate this observation, we designed and co-expressed the GAL4 DNA-binding domain–HDA6 fusion

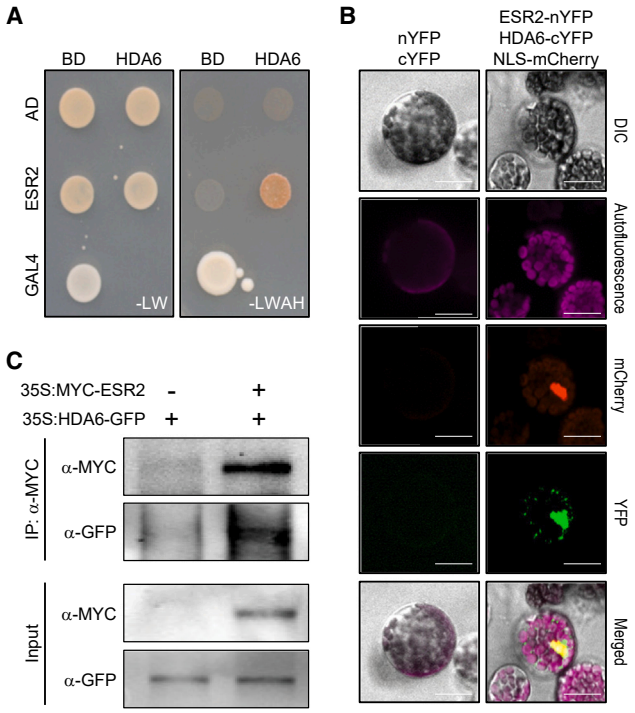

Figure 4. HDA6 interacts with ESR2.

(A) Yeast two-hybrid assays performed using GAL4 DNA-binding domain (BD)-fused HDA6 and GAL4 transcriptional activation domain (AD)-fused ESR2. Interaction between the two proteins was examined by cell growth on selective media. −LWHA: Leu, Trp, His, and Ade dropout plates; −LW: Leu, and Trp dropout plates. GAL4 was used as a positive control.

(B) Bimolecular fluorescence complementation analysis. Partial fragments of yellow fluorescent protein (YFP) fusion constructs containing either HDA6 or ESR2 were transiently co-expressed in *Arabidopsis* protoplasts. The NLS-mCherry construct was used as a nucleus localization marker. Scale bars, 20 μm.

(C) Co-immunoprecipitation assays performed using 2-week-old 35S:*MYC-ESR2* × 35S:*HDA6-GFP* transgenic plants. Epitope-tagged proteins were detected immunologically using anti-GFP and anti-MYC antibodies. IP, immunoprecipitation.

construct with a construct comprising the GAL4 activation domain fused to full-length *ESR2* coding sequence. The co-transformed yeast cells could grow on selective medium, indicating that HDA6 specifically associates with ESR2 (Figure 4A).

To validate the interaction between HDA6 and ESR2 *in vivo*, we performed a bimolecular fluorescence complementation (BiFC) assay. *HDA6* and *ESR2* were translationally fused in frame to the C-terminal fragment of the yellow fluorescent protein (YFP) and the N-terminal fragment of YFP, respectively (Figure 4B). The two constructs were transiently co-expressed in *Arabidopsis* protoplasts. A strong YFP signal was detected primarily in the nucleus of protoplasts expressing the *HDA6-cYFP* and *ESR2-nYFP* combination (Figure 4B), suggesting interaction between HDA6 and ESR2.

Next, the interaction between HDA6 and ESR2 was confirmed *in planta* by a co-immunoprecipitation (co-IP) assay. The 35S:*HDA6-GFP* transgenic plants were crossed with 35S:*MYC-ESR2* transgenic plants, and the total protein extracts of the resulting 35S:*HDA6-GFP* × 35S:*MYC-ESR2* plants were immunoprecipitated with an anti-MYC antibody. Immunoblot analysis with an anti-GFP antibody detected the HDA6 fusion protein (Figure 4C), indicating the interaction between HDA6 and ESR2 *in planta*.

esr2 leaf explants exhibit increased *YUC* expression on 2,4-D-CIM

We postulated that ESR2 is involved in the auxin negative feedback loop and acts with HDA6 to repress *YUC* gene expression. Similar to *HDA6*, the *ESR2* gene was upregulated mainly in the vasculature near the excised regions of leaf explants after 2,4-D application (Figure 5A; Supplemental Figure 17) but did not respond to wounding or cytokinin treatment (Figure 5A). Consistent with the induction of *ESR2* by 2,4-D, *ESR2* expression gradually increased during callus formation on 2,4-D-CIM (Figure 5B). In addition, similar to *hda6-6*, the *YUC1*, *YUC7*, and *YUC9* genes were significantly upregulated in *esr2* leaf explants cultured on 2,4-D-CIM compared with wild type (Figures 3D and 5C; Supplemental Figure 18), whereas the expression of other *YUC*s was unaffected (Supplemental Figure 19). Consistently, free IAA level was also elevated in *esr2* leaf explants compared with wild-type leaf explants cultured on 2,4-D-CIM (Supplemental Figure 20). To further validate the repressive role of ESR2 in auxin biosynthesis during callus initiation, we analyzed β-estradiol-inducible *ESR2*-overexpression transgenic plants (35S:*ESR2-ER*). The expression of *YUC1, YUC7,* and *YUC9* was significantly downregulated in 35S:*ESR2-ER* leaf explants upon β-estradiol treatment (Figure 5D). The *Arabidopsis* genome contains an *ESR2* paralog, *ESR1*. However, *YUC* gene expression was unaffected or downregulated by the mutation of *ESR1* (Supplemental Figure 21), supporting the non-overlapping functions of ESR1 and ESR2 in auxin homeostasis during *in vitro* tissue culture.

To examine whether ESR2, like HDA6, binds directly to *YUC1*, *YUC7*, and *YUC9* loci, we perform a ChIP assay on 35S:*MYC-ESR2* leaf explants cultured on 2,4-D-CIM using an anti-MYC antibody. qPCR analysis of the eluted DNA revealed that ESR2 binds to similar regions of *YUC1*, *YUC7*, and *YUC9* (Figure 5E) as those bound by HDA6 (Figure 3E and 3F). Given that the H3 deacetylation function of HDA6 is likely dependent on ESR2, we examined H3 acetylation levels at *YUC* loci in *esr2* leaf explants. The H3 acetylation levels at *YUC1*, *YUC7*, and *YUC9* loci were substantially elevated in *esr2* leaf explants (Figure 5F), as observed in *hda6-6* leaf explants (Figure 3G). These results indicate that ESR2 and HDA6 co-target the auxin biosynthetic genes to facilitate H3 deacetylation and suppress gene expression.

Consistent with the fact that increased IAA biosynthesis in *hda6-6* mutant leaf explants accelerated cell fate transition and callus initiation on 2,4-D-CIM (Supplemental Figures 13, 14, and 16), cell fate transition was accelerated in *esr2*, along with a rapid induction of *WOX11* and *WOX5* expression (Figure 6A and 6B). Callus formation was also significantly enhanced in *esr2* leaf explants at 14 DAC due to early initiation of callus formation. Fresh weight measurements revealed that the calli derived from *esr2* leaf explants were 26% larger in size than those derived from wild-type leaf explants at 14 DAC (Figure 6C and 6D). Again, *ESR1*, a paralog of *ESR2*, was not involved in callus

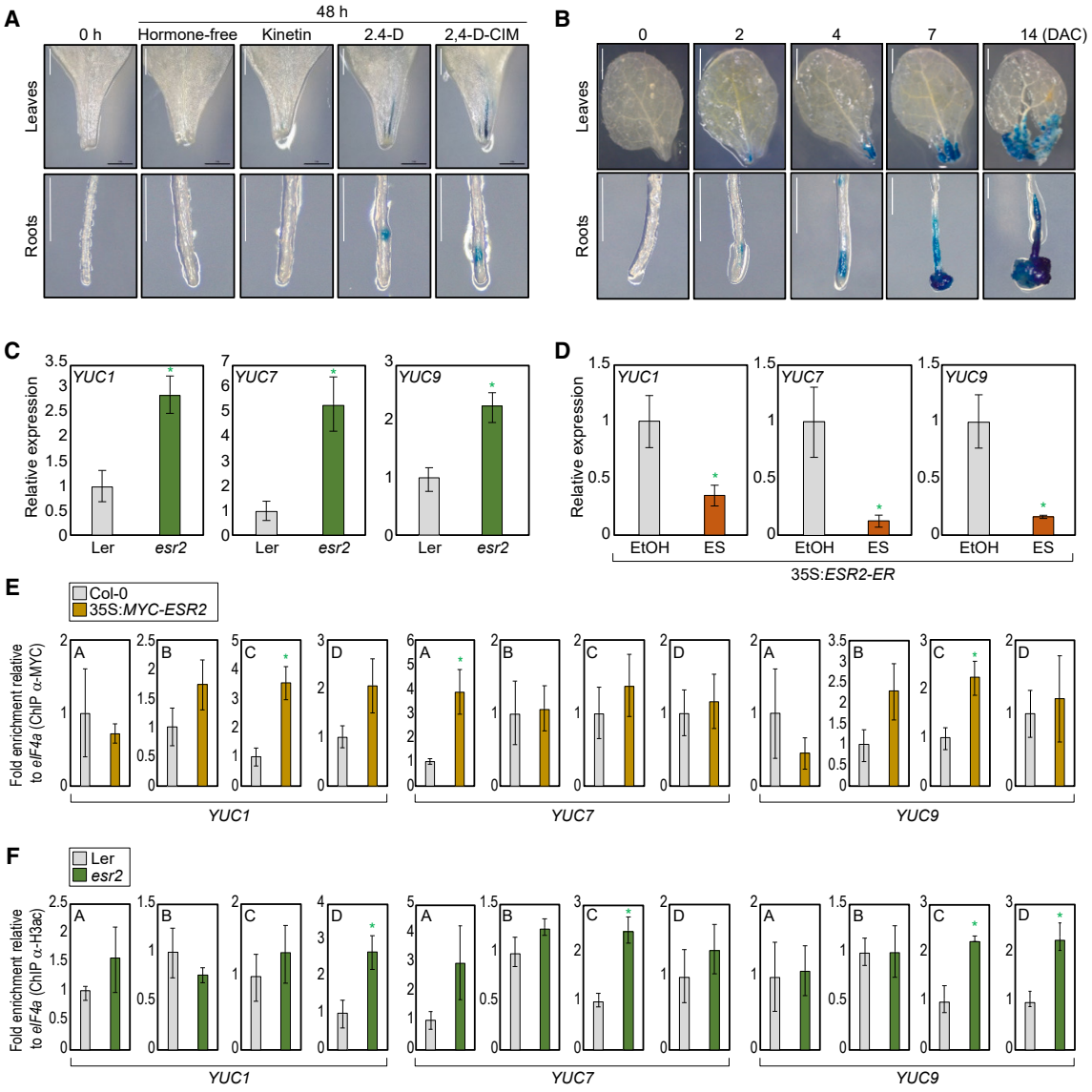

Figure 5. ESR2 directly represses *YUC1*, *YUC7*, and *YUC9* expression.

(A) *ESR2* promoter activity in leaf and root explants of *pESR2::GUS* transgenic plants incubated on culture medium supplemented with kinetin or 2,4-D for 48 h. Scale bars, 1 mm.

(B) *ESR2* promoter activity in leaf and root explants of *pESR2::GUS* transgenic plants cultured on 2,4-D-CIM. DAC, days after incubation on 2,4-D-CIM. Scale bars, 1 mm.

(C) Expression of *YUC* genes in wild-type and *esr2* leaf explants cultured on 2,4-D-CIM for 2 days.

(D) Analysis of β-estradiol-induced changes in *YUC1*, *YUC7*, and *YUC9* expression in leaf explants of 35S:*ESR2-ER* transgenic plants. Leaf explants were incubated on 2,4-D-CIM for 4 days and subsequently on 2,4-D-CIM supplemented with 10 μM β-estradiol for 1 h.

(E) Enrichment of ESR2 on *YUC1*, *YUC7*, and *YUC9* loci.

(F) Abundance of H3ac at *YUC1*, *YUC7*, and *YUC9* loci in wild-type and *esr2* leaf explants, as analyzed by ChIP-qPCR using an anti-H3ac antibody. Data in **(C) to (F)** represent the mean ± SEM of three biological replicates. Asterisks indicate statistically significant differences (*$P < 0.05$; Student's *t*-test).

initiation during *in vitro* tissue culture, as *esr1* leaf explants did not show a significant difference in callus formation phenotypes (Supplemental Figure 21). Given that our results supported the notion that ESR2 negatively regulates auxin biosynthesis on 2,4-D-CIM, which affects cell fate transition, we subsequently investigated whether the increased callus size of *esr2* leaf explants was caused by increased auxin biosynthesis. YDF treatment recovered the enhanced callus phenotype of *esr2* (Figure 6C–6E). Furthermore, earlier cell fate transition in the *esr2* mutant was also compromised by treatment with NPA (Supplemental Figure 22), indicating that the enhanced callus formation of *esr2* was attributable to YUC-directed endogenous auxin biosynthesis as well as polar auxin transport.

To further confirm the role of ESR2 in repressing auxin biosynthesis during callus initiation, we analyzed the callus formation capability of 35S:*ESR2-ER* leaf explants on 2,4-D-CIM. Although wild-type leaf explants were insensitive to

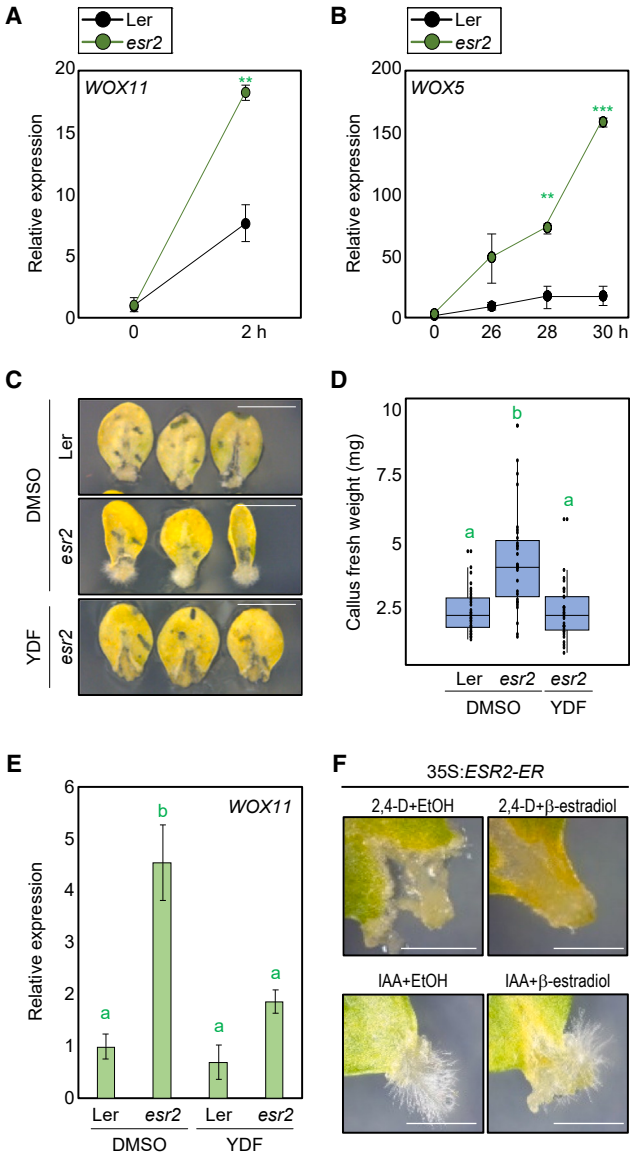

Figure 6. Leaf explants of the *esr2* mutant exhibit early cell fate transition during callus formation.

(A) Real-time RT-qPCR analysis of *WOX11* expression at the wound site of wild-type and *esr2* mutant leaf explants cultured on 2,4-D-CIM for 2 h.

(B) *WOX5* expression at the wound site of wild-type and *esr2* mutant leaf explants cultured on 2,4-D-CIM for up to 30 h. In **(A)** and **(B)**, asterisks indicate statistically significant differences (**$P < 0.01$, ***$P < 0.001$).

(C) Callus phenotype of *esr2* mutant leaf explants incubated on 2,4-D-CIM supplemented with 250 μM YDF for 2 weeks. Scale bars, 5 mm.

(D) Fresh weight of wild-type and *esr2* calli.

(E) *WOX11* expression at the wound site of wild-type and *esr2* mutant leaf explants incubated on 2,4-D-CIM supplemented with 400 μM YDF for 2 h. In **(D)** and **(E)**, statistically significant differences were determined using one-way analysis of variance, followed by Bonferroni's *post hoc* test. Different letters indicate statistically significant differences (*$P < 0.05$).

(F) Callus phenotype of 35S:*ESR2-ER* leaf explants of 2-week-old plants incubated on culture medium (2.25 μM 2,4-D or 2.25 μM IAA) supplemented with 10 μM β-estradiol. Scale bars, 1 mm. Data in **(A), (B), and (E)** represent the mean ± SEM of three biological replicates, whereas data in **(D)** represent box-and-whisker plots.

β-estradiol treatment during callus proliferation, the β-estradiol treatment of 35S:*ESR2-ER* leaf explants completely blocked callus formation at 3 DAC (Figure 6F). In addition, the inhibition of callus initiation observed in β-estradiol-treated 35S:*ESR2-ER* leaf explants could be rescued by IAA supplementation (Figure 6F). These results demonstrate that ESR2, together with HDA6, inhibits auxin biosynthesis in response to high auxin levels, and the negative feedback regulation of auxin biosynthesis delays cell fate transition and callus initiation on 2,4-D-CIM.

ESR2 and HDA6 rely on each other to control *YUC* expression during callus formation

Our findings indicate that ESR2 recruits HDA6 to the *YUC1*, *YUC7*, and *YUC9* loci to repress their expression through H3 deacetylation. To validate the role of ESR2 in the recruitment of HDA6 to *YUC1*, *YUC7*, and *YUC9* loci, we examined the *YUC*-promoter-binding ability of HDA6 in the *esr2* mutant. The 35S:*MYC-HDA6* transgenic plants were crossed with the *esr2* mutant, and the resulting 35S:*MYC-HDA6* × *esr2* plants, which showed HDA6 protein levels comparable to those in 35S:*MYC-HDA6* plants (Supplemental Figure 23), were used for ChIP assays with an anti-MYC antibody. HDA6 showed binding to the *YUC1*, *YUC7*, and *YUC9* loci in wild-type leaf explants on 2,4-D-CIM; however, its binding was substantially diminished in the *esr2* mutant (Figure 7A). Consistently, HDA6-mediated H3 deacetylation of the *YUC1*, *YUC7*, and *YUC9* loci was also impaired in the *esr2* mutant. Specifically, H3ac levels at the *YUC1*, *YUC7*, and *YUC9* loci were reduced in 35S:*HDA6-MYC*-overexpressing protoplasts. However, this reduction in H3ac levels was compromised in 35S:*HDA6-MYC*-overexpressing *esr2* mutant protoplasts (Figure 7B).

Next, we aimed to confirm that HDA6 facilitates H3 deacetylation at the *YUC1*, *YUC7*, and *YUC9* loci. The 35S:*MYC-ESR2* × *hda6-6* plants, which showed ESR2 protein levels comparable to those of the 35S:*MYC-ESR2* plants (Supplemental Figure 23), were generated. HDA6 did not affect the binding of ESR2 to *YUC1*, *YUC7*, and *YUC9* (Figure 7C), as ESR2 is a *bona fide* transcription factor. However, H3ac levels at the three *YUC* loci were significantly reduced in 35S:*MYC-ESR2* leaf explants, by contrast, no reduction in H3ac levels was observed in 35S:*MYC-ESR2* × *hda6-6* leaf explants (Figure 7D). This result was in agreement with *YUC7* expression (Figure 7E). In addition, repression of callus formation by ESR2 was also abolished in 35S:*MYC-ESR2* × *hda6-6* plants (Figure 7F and 7G), indicating that ESR2 and HDA6 are interdependent: ESR2 binds to *YUC* loci and recruits HDA6 to repress *YUC* expression through H3 deacetylation.

The function of ESR2–HDA6 in auxin biosynthesis regulation is not limited to *in vitro* callus initiation but is also likely important for auxin homeostasis during normal growth and development. The negative feedback regulation of auxin biosynthesis by ESR2 and HDA6 was relevant at least in lateral root development, which is known to be under the tight control of endogenous auxin distribution (De Smet et al., 2007; Du and Scheres, 2018). Both *esr2* and *hda6* mutant seedlings displayed increased lateral root density, a phenotype that could be reversed by YDF or NPA treatment (Supplemental Figure 24).

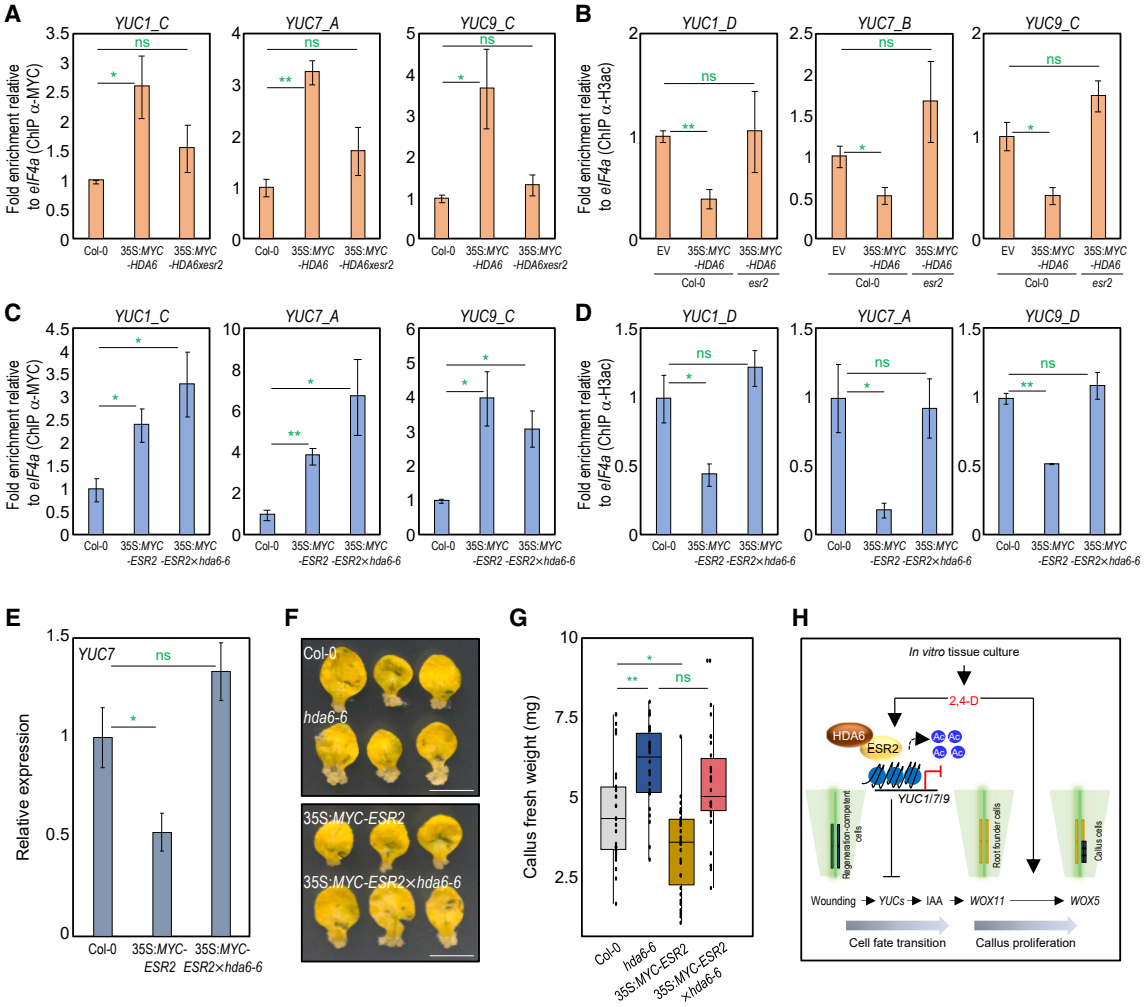

Figure 7. HDA6 and ESR2 function interdependently to regulate *YUC* expression.

(A) Binding of HDA6 to *YUC1*, *YUC7*, and *YUC9* loci in *esr2* mutant leaf explants cultured on 2,4-D-CIM for 2 days. Enrichment of HDA6-binding regions was analyzed by ChIP-qPCR using an anti-MYC antibody.

(B) HDA6-induced H3 deacetylation at *YUC1*, *YUC7*, and *YUC9* loci in the *esr2* mutant. *HDA6* was transiently and ectopically expressed in wild-type and *esr2* mutant protoplasts. Enrichment of H3ac-modified regions was analyzed by ChIP-qPCR using an anti-H3ac antibody. EV, empty vector.

(C) Binding of ESR2 to *YUC1*, *YUC7*, and *YUC9* loci in *hda6-6* mutant leaf explants cultured on 2,4-D-CIM for 2 days. Enrichment of ESR2-binding regions was analyzed by ChIP-qPCR using an anti-MYC antibody.

(D) ESR2-induced H3 deacetylation at *YUC1*, *YUC7*, and *YUC9* loci in *hda6-6* mutant leaf explants cultured on 2,4-D-CIM for 2 days.

(E) *YUC7* expression in leaf explants of 2-week-old wild-type, 35S:*MYC-ESR2*, and 35S:*MYC-ESR2* × *hda6-6* plants incubated on 2,4-D-CIM for 50 min. Data in **(A)–(E)** indicate the mean ± SEM. Asterisks indicate statistically significant differences (*$P < 0.05$, **$P < 0.01$; Student's *t*-test); ns, not significant.

(F) Callus formation in leaf explants of wild-type, *hda6-6*, 35S:*MYC-ESR2*, and *hda6-6* × 35S:*MYC-ESR2* plants incubated on 2,4-D-CIM for 2 weeks. Scale bars, 5 mm.

(G) Fresh weight of wild-type, *hda6-6*, 35S:*MYC-ESR2*, and *hda6-6* × 35S:*MYC-ESR2* calli. The central bar of the box-and-whisker plot represents the median. The upper and lower whiskers represent scores outside the middle 50%. Asterisks indicate statistically significant differences (*$P < 0.05$, **$P < 0.01$; Student's *t*-test); ns, not significant.

(H) Proposed model showing regulation of auxin biosynthesis via a negative feedback loop comprising HDA6 and ESR2. Callus formation from leaf explants and *de novo* root regeneration share the initial process of cellular reprogramming. Upon excision from the plant, the leaf explants exhibit IAA accumulation, which triggers the transition of regeneration-competent cells into root founder cells, possibly by establishing an auxin maximum at the excised region via polar auxin transport. However, the synthetic auxin 2,4-D fails to mimic the action of IAA because of its limited efflux and even decreases IAA biosynthesis via negative feedback regulation, thereby delaying cell fate transition and subsequent callus formation during *in vitro* tissue culture. The negative feedback loop in 2,4-D-CIM-induced calli is mediated by the auxin-inducible HDA6–ESR2 complex, which removes the H3ac mark from *YUC1*, *YUC7*, and *YUC9* loci.

In addition, compared with mock-treated 35S:*ESR2-ER* seedlings, those treated with β-estradiol displayed decreased lateral root number and reduced *YUC* expression levels. However, these defects were rescued by IAA treatment (Supplemental Figure 25). These data suggest that the negative auxin feedback mechanism mediated by the ESR2–HDA6 complex underlies various developmental processes in *Arabidopsis*.

Taken together, these results suggest that ESR2 and HDA6 form a negative feedback circuit to regulate auxin biosynthesis. ESR2 forms a protein complex with HDA6, which then binds to the *YUC1*, *YUC7*, and *YUC9* loci, catalyzing H3 deacetylation to repress their expression. Specifically, auxin biosynthesis is suppressed on 2,4-D-CIM via this negative feedback mechanism, resulting in delayed cell fate transition due to reduced endogenous IAA levels, thereby limiting plant regeneration capacity (Figure 7H).

DISCUSSION

There are two major categories of auxin: natural and synthetic. Natural auxins, such as IAA, phenyl acetic acid, and indole-3-butylic acid, are synthesized by the plant, primarily in the shoot apical meristem, and are then transported basipetally (Flasinski and Hac-Wydro, 2014). Synthetic auxin analogs, such as NAA, 2,4-D, and picloram (Ma et al., 2018), are artificially synthesized. Although these auxin analogs exhibit diverse structures, they share common features such as a planar aromatic ring and a carboxyl side chain, allowing them to be recognized by plant auxin receptors to activate downstream responses (Tan et al., 2007). Accumulating evidence shows that, while natural auxins and synthetic auxin analogs have overlapping functions in the activation of auxin signaling through direct binding to auxin receptors (Kepinski and Leyser, 2005; Calderon-Villalobos et al., 2010), they also have distinct properties, in particular polar transport capability. In contrast to natural auxins, which are transported by both auxin influx and efflux carriers, synthetic auxin analogs have limited transport capabilities. For instance, NAA is actively transported exclusively by auxin efflux carriers, whereas 2,4-D is transported solely by auxin influx carriers (Hosek et al., 2012; Parizkova et al., 2021).

Auxin distribution throughout the plant is delicately regulated by multiple protein families, including AUXIN RESISTANT 1/LIKE AUX, PIN, ATP-BINDING CASSETTE FAMILY B, and PIN-LIKES (Geisler, 2021). They allow directional auxin transport, thereby establishing auxin maxima and/or minima (Blakeslee et al., 2005; Yu et al., 2016). Auxin distribution is essential for various aspects of plant development. For example, an auxin maximum is required for the specification of quiescent center cells and lateral root founder cells in roots (Marhavy et al., 2013; Zhang et al., 2013; Capua and Eshed, 2017). Auxin accumulation is also important for the formation of adventitious roots from excised leaf explants (Chen et al., 2016). Upon leaf excision, IAA, which undergoes polar transport into the excised region of leaf explants, shows significant accumulation within leaf explants (Chen et al., 2016). If auxin distribution is critical for certain biological processes, the role of IAA cannot be replaced by synthetic auxin due to its limited transport ability. Here, we found that the initial process of cell fate transition is likely shared for both *de novo* root regeneration (Liu et al., 2014; Chen et al., 2016) and *in vitro* callus formation (this study) from leaf explants. Upon leaf excision, IAA accumulation at the excised region of leaf explants induces the specification of root founder cells, as evidenced by reduced expression of *WOX11*, a root founder cell marker, in response to inhibitors of auxin biosynthesis or transport (Liu et al., 2014; Chen et al., 2016). In our study, inhibition of endogenous auxin biosynthesis and transport did not lead to callus induction, even in the presence of a high 2,4-D concentration. It is noteworthy that the IAA-dependent cell fate transition was relevant only in leaf explants, whereas IAA biosynthesis and transport had a limited impact on callus initiation from hypocotyl and root explants during *in vitro* tissue culture. These findings are also consistent with the fact that an auxin maximum is established at the excised region after wounding in leaf explants (Chen et al., 2016), while numerous auxin biosynthesis and signaling genes show minimal changes after wounding in hypocotyl explants (Ikeuchi et al., 2017), suggesting that the molecular mechanism underlying cell fate transition could be distinct depending on tissue type.

Endogenous auxin homeostasis is under tight regulation. The activity of YUC enzymes, which convert indole-3-pyruvic acid to IAA, is controlled at multiple levels (Nishimura et al., 2014; Chen et al., 2020), and *YUC* genes are transcriptionally suppressed in response to increased auxin levels via negative feedback regulation, although the underlying molecular mechanism has remained elusive. In this study, we found that the ESR2–HDA6 complex participates in auxin homeostasis regulation. High-concentration auxin treatment, regardless of auxin type (natural or synthetic), activates the transcription of *ESR2* and *HDA6*. The ESR2–HDA6 complex suppresses a subset of *YUC* genes, including *YUC1*, *YUC7*, and *YUC9*, through H3 deacetylation to maintain auxin homeostasis. In *esr2* and *hda6* mutants, *YUC* expression is derepressed in leaf explants on 2,4-D-CIM. The repression of *YUC* genes by the ESR2–HDA6 complex was observed particularly in vascular tissues, where *ESR2* and *HDA6* were expressed in leaf explants cultured on 2,4-D-CIM. Given that IAA-dependent cell fate transition in leaf explants is believed to originate from the procambium or its adjacent parenchyma cells (Liu et al., 2014), the negative feedback mechanism of auxin biosynthesis directly influence the process of cell fate transition upon incubation on 2,4-D-CIM. While our focus was on the impact of the ESR2–HDA6 complex on callus initiation during plant tissue culture, it is important to note that this complex plays a broader role in various aspects of plant development governed by auxin biosynthesis and its homeostasis. For example, balanced endogenous auxin accumulation fine-tunes lateral root emergence (De Smet et al., 2007; Du and Scheres, 2018). An impaired auxin negative feedback loop in *esr2* and *hda6* mutants leads to increased lateral root density. In this context, the *ESR2* and *HDA6* genes likely participate in additional auxin-dependent developmental processes, including wound-induced tissue regeneration, warranting further investigation.

Although 2,4-D is widely used for callus induction, it not only fails to mimic IAA action during callus initiation but also activates the negative feedback circuit that decreases IAA biosynthesis. Considering that IAA is critical for the initial cell fate transition during callus formation, 2,4-D treatment interferes with callus initiation. Indeed, incubation on 2,4-D-CIM repressed *YUC* gene expression and reduced endogenous IAA levels, thereby delaying cell fate transition. Thus, the negative feedback loop inhibiting auxin biosynthesis presents a genetic barrier to callus initiation, because *in vitro* tissue culture intrinsically requires exogenous auxin application at a high concentration. This genetic hurdle could be overcome by suppressing HDA6 and ESR2 activities. The negative feedback loop was impaired in *hda6* and *esr2* mutants, which consequently showed rapid auxin biosynthesis and enhanced root founder cell specification, leading to accelerated

callus initiation even at high 2,4-D concentrations. Considering the conservation of the *HDA6* and *ESR2* genes across various plant species (Xu et al., 2021; Niu et al., 2022), our findings hold promise for improving tissue culture efficiency in a broad array of crop species.

Despite the negative impact of 2,4-D on cell fate transition, 2,4-D is still widely used in *in vitro* tissue culture for the following reasons. First, in several plant species, including *Arabidopsis,* endogenous auxin is produced at a biologically relevant level even in the presence of a certain amount of 2,4-D, as the negative feedback loop does not completely block auxin biosynthesis. Notably, although callus initiation was significantly delayed, cell fate transition eventually occurred in leaf explants on 2,4-D-CIM. Second, after cell fate transition, active callus proliferation is essential for pluripotency acquisition, a process more effectively induced by 2,4-D than by IAA (Supplemental Figure 26). Synthetic auxins, such as 2,4-D, demonstrate greater stability than natural auxins like IAA, thus promoting cell proliferation more effectively. The delayed cell fate transition can also sometimes be compensated for by prolonged incubation on 2,4-D-CIM. Based on these results, we propose that callus formation can be further enhanced by a two-step callus induction process involving cell fate transition on IAA-containing medium, followed by callus proliferation on 2,4-D-containing medium. This method would be particularly beneficial for monocots and woody plants, which typically exhibit low callus formation ability due to their limited callus initiation capacity (Hu et al., 2017).

METHODS

Plant materials and growth conditions

A. thaliana ecotype Columbia-0 was used for all experiments, unless otherwise specified. Plants were grown under long-day conditions (16-h light/8-h dark cycles) with white fluorescent light (120 μmol photons m^{-2} s^{-1}) at 22°C–23°C. The *drn-1/esr1*, *drnl-2/esr2*, *hda6-6*, *pESR2::GUS*, 35S:*ESR2-ER*, *pHDA6::HDA6-GFP/hda6-6*, 35S:*HDA6-GFP/hda6-6*, *pARF7::GUS*, *pYUC9::GUS*, and *pWOX11::GUS* plants have been described previously (Chandler et al., 2007; Chen et al., 2016; Yu et al., 2017a; Duran-Medina et al., 2017; Lee et al., 2019; Shin et al., 2022). The *yuc2589* (CS69869) and *pYUC7::eGFP-GUS* (CS69896) seeds were obtained from the Arabidopsis Biological Resource Center.

To induce callus formation, leaf explants of 2-week-old plants were incubated on 2,4-D-CIM (MS medium supplemented with 3% [w/v] sucrose, 2.2 μM 2,4-D, and 0.2 μM kinetin), followed by incubation at 22°C in darkness. YDF, a potent inhibitor of plant YUC enzymes, was obtained from Dr. Hayashi Kenichiro (Department of Biochemistry, Okayama University of Science, Okayama, Japan) and used at a final concentration of 200–400 μM. To perform the β-estradiol experiment, leaf explants prepared from the third and fourth leaves of 2-week-old 35S:*ESR2-ER* plants were incubated on culture medium supplemented with 10 μM β-estradiol (Sigma-Aldrich).

Real-time RT-qPCR analysis

Total RNA extraction and real-time reverse-transcription (RT)-qPCR were performed as described previously (Lee et al., 2021). RT was performed using Moloney murine leukemia virus reverse transcriptase (Enzynomics) and dT20 oligos to synthesize first-strand cDNA from 2 μg of total RNA. The cDNAs were diluted to 100 μl with Tris–EDTA buffer, and 1 μl of the diluted cDNA was used for PCR amplification. Real-time RT-qPCR was performed in a 96-well block using the Step-One Plus real-time PCR system (Applied Biosystems) and sequence-specific PCR primers (Supplemental Table 1). Values corresponding to target genes were normalized relative to the *EUKARYOTIC TRANSLATION INITIATION FACTOR 4A1* (*eIF4A*) gene (At3g13920). Each PCR amplification was performed using total RNA extracted from three independent biological replicates. The comparative $\Delta\Delta C_T$ method was employed to evaluate the relative quantity of each amplified product. The threshold cycle (C_T) for each reaction was determined automatically using analysis software with default parameters. The specificity of each reaction was determined by analyzing the melting curve of each amplified product.

Histochemical staining

The *pARF7::GUS*, *pESR2::GUS*, *pYUC7::eGFP-GUS*, *pYUC9::GUS*, and *pWOX11::GUS* leaf explants were fixed by immersing in 90% (v/v) acetone for 20 min on ice and then washed twice with rinsing solution (50 mM sodium phosphate [pH 7.0], 0.5 mM $K_3Fe(CN)_6$, and 0.5 mM $K_4Fe(CN)_6$). The fixed samples were subsequently incubated in staining solution containing 1 mM 5-bromo-4-chloro-3-indolyl-β-d-glucuronide (Duchefa) at 37°C for 5 h. The stained tissues were clarified by incubating in chloral hydrate solution as described previously (Liu et al., 2014).

ChIP assay

The ChIP assay was performed as reported previously (Kuhn and Ostergaard, 2020), with some modifications. In brief, all plant samples were cross-linked with 1% formaldehyde (w/v), ground to a fine powder in liquid nitrogen, and sonicated. The sonicated chromatin complexes were precipitated with salmon sperm DNA/protein A agarose beads (Millipore) and then incubated with anti-MYC (05-724; Millipore) and anti-H3ac (06-599; Millipore) antibodies. The precipitated DNA fragments were quantified by real-time qPCR using sequence-specific primers (Supplemental Table 2). Values were normalized relative to the *eIF4a* gene.

Y2H assay

The full-length HDA6 coding sequence (CDS) was cloned into the pGBKT7 vector to generate the bait vector. The bait construct was co-transformed into yeast (*Saccharomyces cerevisiae*) strain PJG694a harboring *LacZ* and *histidine* (*His*) reporter genes, with a prey cDNA library (630487; Takara) according to the manufacturer's instructions. Positive yeast clones were selected in SD medium lacking Leu, Trp, His, and adenine (SD/−Leu/−Trp/−His/−Ade). Subsequently, the gene inserts from positive colonies were sequenced and identified using BLAST. To confirm protein–protein interactions, the full-length *ESR2* CDS was cloned into pGADT7, and the resulting construct was used as the prey vector in Y2H assays. The prey and bait constructs were co-transformed into yeast strain PJG694a. The transformed yeast cells were selected by growth on SD/−Leu/−Trp, and protein–protein interactions were tested on SD/−Leu/−Trp/−His/−Ade. Full-length *GAL4* was expressed as a positive control (Clontech).

BiFC assay

The BiFC assay was performed as described previously (Lee et al., 2021). Full-length *ESR2* and *HDA6* CDSs were fused in frame to the 5′ end of a gene sequence encoding the N-terminal half of firefly EYFP or the C-terminal half of EYFP, respectively. The mCherry construct was used as a nucleus localization marker. The recombinant constructs were co-transfected into *Arabidopsis* mesophyll protoplasts by the polyethylene glycol–calcium transfection method (Yoo et al., 2007). Transformed protoplasts were incubated at 23°C for 12–16 h in darkness. Fluorescence signals were monitored using a CQ1 confocal microscope (Yokogawa).

Co-IP assay

To perform the co-IP assay, 35S:*HDA6-GFP* transgenic plants were crossed with 35S:*MYC-ESR2* transgenic plants. Two-week-old *Arabidopsis* seedlings were homogenized in liquid nitrogen, and total protein was extracted using protein extraction buffer (25 mM Tris–HCl [pH 7.5], 150 mM NaCl, 5% glycerol [v/v], 0.05% Nonidet P-40 [v/v], 2.5 mM EDTA, 1

mM phenylmethylsulfonyl fluoride, and 1× protease inhibitor cocktail). Five percent of each extract was reserved for use as the input (control). Immunoprecipitation was performed using an anti-MYC antibody (05-724; Millipore) coupled with protein A/G Sepharose beads (Santa Cruz Biotechnology), followed by washing at least four times with protein extraction buffer. To elute and electrophorese the proteins, the samples were mixed with 2× sodium dodecyl sulfate (SDS)–polyacrylamide gel electrophoresis (PAGE) loading buffer and subjected to SDS–PAGE, followed by immunodetection with an anti-MYC or anti-GFP antibody (ab290; Abcam).

Immunoblot analysis

Plant materials were ground in liquid nitrogen, and total protein was suspended in SDS–PAGE loading buffer. The samples were then loaded onto a 10% polyacrylamide gel and separated by SDS–PAGE as described previously (Lee et al., 2021). Proteins in the gel were blotted onto Hybond-P+ membranes (Amersham Pharmacia). Epitope-tagged proteins were immunologically detected using an anti-GFP antibody.

Measurement of free IAA content

Leaf explants cultured on 2,4-D-CIM or 2,4-D-depleted CIM for 1 day were harvested for the extraction of free IAA. Approximately 0.1 g of ground plant material was mixed with 1 ml of ethyl acetate–formic acid solution (99.5:0.5) containing 20 ng of D5-IAA as an internal standard. The samples were mixed vigorously for 1 min and centrifuged at 13 000 rpm for 20 min at 4°C. The supernatants were transferred into a new 2-ml centrifuge tube, and the previous process was repeated by adding 0.5 ml of ethyl acetate–formic acid solution without internal standards, and then the supernatants were combined. The supernatants were evaporated at room temperature in a SpeedVac (Thermo Fisher Scientific). The pellets were resuspended in 500 μl of methanol–water solution (70:30) and centrifuged at 13 000 rpm for 10 min. The 400-μl supernatants were transferred into a vial. The IAA content was measured using liquid chromatography–mass spectrometry (LCMS-8050, Shimadzu).

Statistical analysis

Statistical analysis of all data was conducted using GraphPad Prism 8 software.

SUPPLEMENTAL INFORMATION

Supplemental information is available at *Plant Communications Online*.

FUNDING

This work was supported by the Basic Science Research (NRF-2022R1A2B5B02001266) and Basic Research Laboratory (NRF-2022R1A4A3024451) programs funded by the National Research Foundation of Korea (South Korea) and the New Breeding Technologies Development Program (RS-2024-00322275) of the Rural Development Administration (South Korea).

AUTHOR CONTRIBUTIONS

P.J.S. conceived the study, and K.L. designed the research. K.L., H.Y., and O.-S.P. conducted the experiments. J.L. and S.-G.K. conducted auxin measurements. P.J.S. wrote the manuscript in discussion with K.L. All authors read and approved the manuscript.

ACKNOWLEDGMENTS

We thank Dr. John Chandler (Cologne University, Germany) for kindly providing *drn-1* seeds; Dr. Nayelli Marsch-Martínez (Unidad Irapuato, Mexico) for providing *drnl-2*, *pESR2::GUS*, and 35S:*ESR2-ER* seeds; Dr. Keqiang Wu (National Taiwan University, Taiwan) for providing *pHDA6::HDA6-GFP/hda6-6* and 35S:*HDA6-GFP/hda6-6* seeds; Dr. Jungmook Kim (Chonnam National University, Korea) for providing *pARF7::GUS*; Dr. Lin Xu (Chinese Academy of Sciences, China) for providing *pYUC9::GUS*; Dr. Hyo-Jun Lee (Korea Research Institute of Bioscience and Biotechnology, Korea) for providing *pWOX11::GUS*; and Dr. Hayashi Kenichiro (Okayama University of Science, Japan) for providing YDF. No conflict of interest is declared.

Received: August 10, 2023
Revised: March 27, 2024
Accepted: April 1, 2024
Published: April 2, 2024

REFERENCES

Bai, B., Su, Y.H., Yuan, J., and Zhang, X.S. (2013). Induction of somatic embryos in *Arabidopsis* requires local YUCCA expression mediated by the down-regulation of ethylene biosynthesis. Mol. Plant **6**:1247–1260.

Blakeslee, J.J., Peer, W.A., and Murphy, A.S. (2005). Auxin transport. Curr. Opin. Plant Biol. **8**:494–500.

Boccaccini, A., Legris, M., Krahmer, J., Allenbach-Petrolati, L., Goyal, A., Galvan-Ampudia, C., Vernoux, T., Karayekov, E., Casal, J.J., and Fankhauser, C. (2020). Low blue light enhances phototropism by releasing cryptochrome1-mediated inhibition of *PIF4* expression. Plant Physiol. **183**:1780–1793.

Cai, X.T., Xu, P., Zhao, P.X., Liu, R., Yu, L.H., and Xiang, C.B. (2014). *Arabidopsis* ERF109 mediates cross-talk between jasmonic acid and auxin biosynthesis during lateral root formation. Nat. Commun. **5**:5833.

Calderon-Villalobos, L.I., Tan, X., Zheng, N., and Estelle, M. (2010). Auxin perception–structural insights. Cold Spring Harbor Perspect. Biol. **2**:a005546.

Cao, X., Yang, H., Shang, C., Ma, S., Liu, L., and Cheng, J. (2019). The roles of auxin biosynthesis *YUCCA* gene family in plants. Int. J. Mol. Sci. **20**, 6343.

Capua, Y., and Eshed, Y. (2017). Coordination of auxin-triggered leaf initiation by tomato LEAFLESS. Proc. Natl. Acad. Sci. USA **114**:3246–3251.

Challa, K.R., Aggarwal, P., and Nath, U. (2016). Activation of *YUCCA5* by the transcription factor TCP4 integrates developmental and environmental signals to promote hypocotyl elongation in *Arabidopsis*. Plant Cell **28**:2117–2130.

Chandler, J.W., Cole, M., Flier, A., Grewe, B., and Werr, W. (2007). The AP2 transcription factors DORNROSCHEN and DORNROSCHEN-LIKE redundantly control *Arabidopsis* embryo patterning via interaction with PHAVOLUTA. Development **134**:1653–1662.

Che, P., Lall, S., and Howell, S.H. (2007). Developmental steps in acquiring competence for shoot development in *Arabidopsis* tissue culture. Planta **226**:1183–1194.

Chen, L., Tong, J., Xiao, L., Ruan, Y., Liu, J., Zeng, M., Huang, H., Wang, J.W., and Xu, L. (2016). YUCCA-mediated auxin biogenesis is required for cell fate transition occurring during de novo root organogenesis in Arabidopsis. J. Exp. Bot. **67**:4273–4284.

Chen, L., Huang, X.X., Zhao, S.M., Xiao, D.W., Xiao, L.T., Tong, J.H., Wang, W.S., Li, Y.J., Ding, Z., and Hou, B.K. (2020). IPyA glucosylation mediates light and temperature signaling to regulate auxin-dependent hypocotyl elongation in *Arabidopsis*. Proc. Natl. Acad. Sci. USA **117**:6910–6917.

De Smet, I., Tetsumura, T., De Rybel, B., Frei dit Frey, N., Laplaze, L., Casimiro, I., Swarup, R., Naudts, M., Vanneste, S., Audenaert, D., et al. (2007). Auxin-dependent regulation of lateral root positioning in the basal meristem of Arabidopsis. Development **134**:681–690.

Du, Y., and Scheres, B. (2018). Lateral root formation and the multiple roles of auxin. J. Exp. Bot. **69**:155–167.

Durán-Medina, Y., Serwatowska, J., Reyes-Olalde, J.I., de Folter, S., and Marsch-Martínez, N. (2017). The AP2/ERF transcription factor DRNL modulates gynoecium development and affects its response to cytokinin. Front. Plant Sci. **8**:1841.

Fan, M., Xu, C., Xu, K., and Hu, Y. (2012). LATERAL ORGAN BOUNDARIES DOMAIN transcription factors direct callus formation in *Arabidopsis* regeneration. Cell Res. **22**:1169–1180.

Flasiński, M., and Hąc-Wydro, K. (2014). Natural vs synthetic auxin: studies on the interactions between plant hormones and biological membrane lipids. Environ. Res. **133**:123–134.

Geisler, M.M. (2021). A retro-perspective on auxin transport. Front. Plant Sci. **12**, 756968.

Ghanbari, S., Fakheri, B.A., Naghavi, M.R., and Mahdinezhad, N. (2018). New protocol for the indirect regeneration of the Lilium ledebourii Bioss by using bulb explants. J. Plant Biotechnol. **45**:146–153.

Hosek, P., Kubes, M., Lanková, M., Dobrev, P.I., Klíma, P., Kohoutová, M., Petrásek, J., Hoyerová, K., Jirina, M., and Zazímalová, E. (2012). Auxin transport at cellular level: new insights supported by mathematical modelling. J. Exp. Bot. **63**:3815–3827.

Hu, B., Zhang, G., Liu, W., Shi, J., Wang, H., Qi, M., Li, J., Qin, P., Ruan, Y., Huang, H., et al. (2017). Divergent regeneration-competent cells adopt a common mechanism for callus initiation in angiosperms. Regeneration (Oxf) **4**:132–139.

Hu, X., and Xu, L. (2016). Transcription factors WOX11/12 directly cctivate *WOX5/7* to promote root primordia initiation and organogenesis. Plant Physiol. **172**:2363–2373.

Ikeda, Y., Banno, H., Niu, Q.W., Howell, S.H., and Chua, N.H. (2006). The ENHANCER OF SHOOT REGENERATION 2 gene in *Arabidopsis* regulates *CUP-SHAPED COTYLEDON 1* at the transcriptional level and controls cotyledon development. Plant Cell Physiol. **47**:1443–1456.

Ikeda, Y., Králová, M., Zalabák, D., Kubalová, I., and Aida, M. (2021). Post-embryonic lateral organ development and adaxial-abaxial polarity are regulated by the combined effect of ENHANCER OF SHOOT REGENERATION 1 and WUSCHEL in *Arabidopsis* Shoots. Int. J. Mol. Sci. **22**, 10621.

Ikeuchi, M., Rymen, B., and Sugimoto, K. (2020). How do plants transduce wound signals to induce tissue repair and organ regeneration? Curr. Opin. Plant Biol. **57**:72–77.

Ikeuchi, M., Iwase, A., Rymen, B., Lambolez, A., Kojima, M., Takebayashi, Y., Heyman, J., Watanabe, S., Seo, M., De Veylder, L., et al. (2017). Wounding triggers callus formation via dynamic hormonal and transcriptional changes. Plant Physiol. **175**:1158–1174.

Iwase, A., Harashima, H., Ikeuchi, M., Rymen, B., Ohnuma, M., Komaki, S., Morohashi, K., Kurata, T., Nakata, M., Ohme-Takagi, M., et al. (2017). WIND1 promotes shoot regeneration through transcriptional activation of *ENHANCER OF SHOOT REGENERATION1* in *Arabidopsis*. Plant Cell **29**:54–69.

Kareem, A., Durgaprasad, K., Sugimoto, K., Du, Y., Pulianmackal, A.J., Trivedi, Z.B., Abhayadev, P.V., Pinon, V., Meyerowitz, E.M., Scheres, B., et al. (2015). *PLETHORA* genes control regeneration by a two-step mechanism. Curr. Biol. **25**:1017–1030.

Kepinski, S., and Leyser, O. (2005). The *Arabidopsis* F-box protein TIR1 is an auxin receptor. Nature **435**:446–451.

Kuhn, A., and Østergaard, L. (2020). Chromatin Immunoprecipitation (ChIP) to assess histone marks in auxin-treated *Arabidopsis thaliana* inflorescence tissue. Bio. Protoc. **10**, e3832.

Lee, H.W., Cho, C., Pandey, S.K., Park, Y., Kim, M.J., and Kim, J. (2019). *LBD16* and *LBD18* acting downstream of ARF7 and ARF19 are involved in adventitious root formation in *Arabidopsis*. BMC Plant Biol. **19**:46.

Lee, K., Park, O.S., Go, J.Y., Yu, J., Han, J.H., Kim, J., Bae, S., Jung, Y.J., and Seo, P.J. (2021). *Arabidopsis* ATXR2 represses *de novo* shoot organogenesis in the transition from callus to shoot formation. Cell Rep. **37**, 109980.

Liu, J., Hu, X., Qin, P., Prasad, K., Hu, Y., and Xu, L. (2018). The WOX11-LBD16 pathway promotes pluripotency acquisition in callus cells during *de novo* shoot Regeneration in tissue culture. Plant Cell Physiol. **59**:734–743.

Liu, J., Sheng, L., Xu, Y., Li, J., Yang, Z., Huang, H., and Xu, L. (2014). WOX11 and 12 are involved in the first-step cell fate transition during *de novo* root organogenesis in *Arabidopsis*. Plant Cell **26**:1081–1093.

Liu, W., Zhang, Y., Fang, X., Tran, S., Zhai, N., Yang, Z., Guo, F., Chen, L., Yu, J., Ison, M.S., et al. (2022). Transcriptional landscapes of de novo root regeneration from detached Arabidopsis leaves revealed by time-lapse and single-cell RNA sequencing analyses. Plant Commun. **3**, 100306.

Ma, Q., Grones, P., and Robert, S. (2018). Auxin signaling: a big question to be addressed by small molecules. J. Exp. Bot. **69**:313–328.

Marhavý, P., Vanstraelen, M., De Rybel, B., Zhaojun, D., Bennett, M.J., Beeckman, T., and Benková, E. (2013). Auxin reflux between the endodermis and pericycle promotes lateral root initiation. EMBO J. **32**:149–158.

Matiolli, C.C., and Melotto, M. (2018). A comprehensive Arabidopsis yeast two-hybrid library for protein-protein interaction studies: a resource to the plant research community. Mol. Plant Microbe Interact. **31**:899–902.

Matsuo, N., Makino, M., and Banno, H. (2011). *Arabidopsis* ENHANCER OF SHOOT REGENERATION (ESR)1 and ESR2 regulate *in vitro* shoot regeneration and their expressions are differentially regulated. Plant Sci. **181**:39–46.

Meng, W.J., Cheng, Z.J., Sang, Y.L., Zhang, M.M., Rong, X.F., Wang, Z.W., Tang, Y.Y., and Zhang, X.S. (2017). Type-B ARABIDOPSIS RESPONSE REGULATORs specify the shoot stem cell niche by dual regulation of *WUSCHEL*. Plant Cell **29**:1357–1372.

Nag, A., Yang, Y., and Jack, T. (2007). *DORNROSCHEN-LIKE*, an AP2 gene, is necessary for stamen emergence in *Arabidopsis*. Plant Mol. Biol. **65**:219–232.

Nishimura, T., Hayashi, K.I., Suzuki, H., Gyohda, A., Takaoka, C., Sakaguchi, Y., Matsumoto, S., Kasahara, H., Sakai, T., Kato, J.I., et al. (2014). Yucasin is a potent inhibitor of YUCCA, a key enzyme in auxin biosynthesis. Plant J. **77**:352–366.

Niu, H., Wang, H., Zhao, B., He, J., Yang, L., Ma, X., Cao, J., Li, Z., and Shen, J. (2022). Exogenous auxin-induced ENHANCER OF SHOOT REGENERATION 2 (ESR2) enhances femaleness of cucumber via activating *CsACS2* gene. Hortic. Res. **9**, uhab085.

Ohbayashi, I., Sakamoto, Y., Kuwae, H., Kasahara, H., and Sugiyama, M. (2022). Enhancement of shoot regeneration by treatment with inhibitors of auxin biosynthesis and transport during callus induction in tissue culture of *Arabidopsis thaliana*. Plant Biotechnol. **39**:43–50.

Pařízková, B., Žukauskaitė, A., Vain, T., Grones, P., Raggi, S., Kubeš, M.F., Kieffer, M., Doyle, S.M., Strnad, M., Kepinski, S., et al. (2021). New fluorescent auxin probes visualise tissue-specific and subcellular distributions of auxin in *Arabidopsis*. New Phytol. **230**:535–549.

Shin, J., and Seo, P.J. (2018). Varying auxin levels induce distinct pluripotent states in callus cells. Front. Plant Sci. **9**:1653.

Shin, S.Y., Park, S.J., Kim, H.S., Jeon, J.H., and Lee, H.J. (2022). Wound-induced signals regulate root organogenesis in Arabidopsis explants. BMC Plant Biol. **22**:133.

Sussex, I.M. (2008). The scientific roots of modern plant biotechnology. Plant Cell **20**:1189–1198.

Suzuki, M., Yamazaki, C., Mitsui, M., Kakei, Y., Mitani, Y., Nakamura, A., Ishii, T., Soeno, K., and Shimada, Y. (2015). Transcriptional feedback regulation of *YUCCA* genes in response to auxin levels in *Arabidopsis*. Plant Cell Rep. **34**:1343–1352.

Tan, X., Calderon-Villalobos, L.I.A., Sharon, M., Zheng, C., Robinson, C.V., Estelle, M., and Zheng, N. (2007). Mechanism of auxin perception by the TIR1 ubiquitin ligase. Nature **446**:640–645.

Teale, W., and Palme, K. (2018). Naphthylphthalamic acid and the mechanism of polar auxin transport. J. Exp. Bot. **69**:303–312.

Temman, H., Sakamoto, T., Ueda, M., Sugimoto, K., Migihashi, M., Yamamoto, K., Tsujimoto-Inui, Y., Sato, H., Shibuta, M.K., Nishino, N., et al. (2023). Histone deacetylation regulates de novo shoot regeneration. PNAS Nexus **2**, pgad002.

Tsugafune, S., Mashiguchi, K., Fukui, K., Takebayashi, Y., Nishimura, T., Sakai, T., Shimada, Y., Kasahara, H., Koshiba, T., and Hayashi, K.I. (2017). Yucasin DF, a potent and persistent inhibitor of auxin biosynthesis in plants. Sci. Rep. **7**, 13992.

Wójcikowska, B., Botor, M., Morończyk, J., Wójcik, A.M., Nodzyński, T., Karcz, J., and Gaj, M.D. (2018). Trichostatin A triggers an embryogenic transition in *Arabidopsis* explants via an auxin-related pathway. Front. Plant Sci. **9**:1353.

Xu, C., Cao, H., Zhang, Q., Wang, H., Xin, W., Xu, E., Zhang, S., Yu, R., Yu, D., and Hu, Y. (2018). Control of auxin-induced callus formation by bZIP59-LBD complex in *Arabidopsis* regeneration. Nat. Plants **4**:108–115.

Xu, Q., Liu, Q., Chen, Z., Yue, Y., Liu, Y., Zhao, Y., and Zhou, D.X. (2021). Histone deacetylases control lysine acetylation of ribosomal proteins in rice. Nucleic Acids Res. **49**:4613–4628.

Yu, C.W., Liu, X., Luo, M., Chen, C., Lin, X., Tian, G., Lu, Q., Cui, Y., and Wu, K. (2011). HISTONE DEACETYLASE6 interacts with FLOWERING LOCUS D and regulates flowering in *Arabidopsis*. Plant Physiol. **156**:173–184.

Yu, C.W., Tai, R., Wang, S.C., Yang, P., Luo, M., Yang, S., Cheng, K., Wang, W.C., Cheng, Y.S., and Wu, K. (2017a). HISTONE DEACETYLASE6 acts in concert with histone methyltransferases SUVH4, SUVH5, and SUVH6 to regulate transposon silencing. Plant Cell **29**:1970–1983.

Yoo, S.D., Cho, Y.H., and Sheen, J. (2007). Arabidopsis mesophyll protoplasts: a versatile cell system for transient gene expression analysis. Nat Protoc **2**:1565–1572.

Yu, J., Liu, W., Liu, J., Qin, P., and Xu, L. (2017b). Auxin control of root organogenesis from callus in tissue culture. Front. Plant Sci. **8**:1385.

Yu, Q., Zhang, Y., Wang, J., Yan, X., Wang, C., Xu, J., and Pan, J. (2016). Clathrin-mediated auxin efflux and maxima regulate hypocotyl hook formation and light-stimulated hook opening in *Arabidopsis*. Mol. Plant **9**:101–112.

Zhang, W., Swarup, R., Bennett, M., Schaller, G.E., and Kieber, J.J. (2013). Cytokinin induces cell division in the quiescent center of the *Arabidopsis* root apical meristem. Curr. Biol. **23**:1979–1989.

Zhao, Y., Hull, A.K., Gupta, N.R., Goss, K.A., Alonso, J., Ecker, J.R., Normanly, J., Chory, J., and Celenza, J.L. (2002). Trp-dependent auxin biosynthesis in *Arabidopsis*: involvement of cytochrome P450s CYP79B2 and CYP79B3. Genes Dev. **16**:3100–3112.